Sunlight-Driven Nitrate-to-Ammonia Reduction with Water by Iron Oxyhydroxide Photocatalysts

Yasuhiro Shiraishi,* Shotaro Akiyama, Wataru Hiramatsu, Kazutoshi Adachi, Satoshi Ichikawa, and Takayuki Hirai

Read Online

ACCESS | Metrics & More | Article Recommendations | Supporting Information

ABSTRACT: The photocatalytic reduction of harmful nitrates (NO_3^-) in strongly acidic wastewater to ammonia (NH_3) under sunlight is crucial for the recycling of limited nitrogen resources. This study reports that a naturally occurring Cl^--containing iron oxyhydroxide (akaganeite) powder with surface oxygen vacancies $(\beta\text{-FeOOH(Cl)-OVs})$ facilitates this transformation. Ultraviolet light irradiation of the catalyst suspended in a Cl^--containing solution promoted quantitative NO_3^--to-NH_3 reduction with water under ambient conditions. The photogenerated conduction band electrons promoted the reduction of NO_3^--to-NH_3 over the OVs. The valence band holes promoted self-oxidation of Cl^- as the direct electron donor and eliminated Cl^- was compensated from the

solution. Photodecomposition of the generated hypochlorous acid (HClO) produced O_2, facilitating catalytic reduction of NO_3^--to-NH_3 with water as the electron donor in the entire system. Simulated sunlight irradiation of the catalyst in a strongly acidic nitric acid (HNO_3) solution $(pH \sim 1)$ containing Cl^- stably generated NH_3 with a solar-to-chemical conversion efficiency of $\sim 0.025\%$. This strategy paves the way for sustainable NH_3 production from wastewater.

KEYWORDS: photocatalysis, nitrate, ammonia, ion oxyhydroxide, artificial photosynthesis
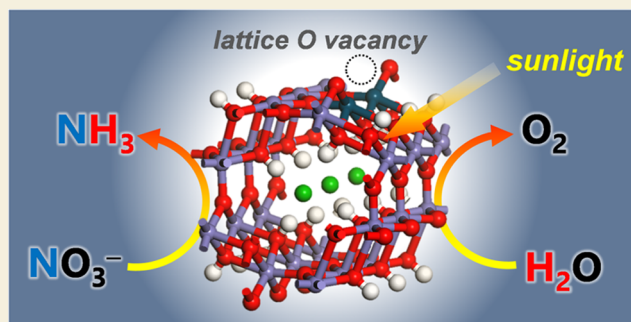
INTRODUCTION

Ammonia (NH_3) is an irreplaceable chemical to produce fertilizers, pharmaceuticals, and fibers.[1] Moreover, it has attracted increasing attention as a hydrogen carrier for the development of a sustainable energy society.[2] For more than a century, NH_3 has been manufactured using the Haber−Bosch process via the reduction of nitrogen (N_2) with hydrogen (H_2). This process requires high-pressure (>200 bar) and high-temperature (>673 K) conditions, utilizes a large amount of H_2 produced by the steam reforming of fossil fuels, and inevitably causes a large concomitant emission of CO_2.[3] As an attractive alternative to this process, electrocatalytic and photocatalytic processes have received considerable attention over the past few years because they can facilitate the N_2-to-NH_3 transformation under ambient pressure and temperature conditions without the use of H_2.[4−6] However, owing to the extremely stable $N\equiv N$ bond of N_2 (941 kJ mol^{-1}),[7] these processes suffer from low activity despite significant progress in catalyst development. Therefore, the use of N_2 gas as a N source for electrocatalytic/photocatalytic NH_3 generation requires extensive development for practical applications.

Nitrates (NO_3^-) are one of the most widespread water pollutants. Its absorption causes several diseases such as methemoglobinemia and non-Hodgkin's lymphoma;[8] therefore, the maximum permissive level of NO_3^- in drinking water

is set at 45 ppm by the World Health Organization (WHO).[9] A large amount of NO_3^- is emitted from various sources including industrial wastewater, nuclear waste, livestock excrement, and chemical fertilizers with a wide concentration range (up to ~ 2 M).[10] The wastewater is usually strongly acidic; therefore, neutralization by an alkali treatment followed by biological reduction of NO_3^- into N_2 using anaerobic bacteria is required before discharging.[11] Currently, NO_3^- is considered a potential N source for practical NH_3 production[12,13] because of its high emission and low dissociation energy of its $N\!=\!O$ bond (204 kJ mol^{-1}).[14] Recent developments of electrocatalysts achieved NO_3^--to-NH_3 reduction with more than 75% Faradaic efficiency under a relatively low applied voltage of about −0.5 V vs a reversible hydrogen electrode (RHE).[15−17] However, these systems required neutral−basic solutions by neutralization to suppress the H_2 evolution reaction.
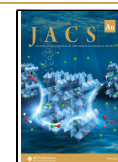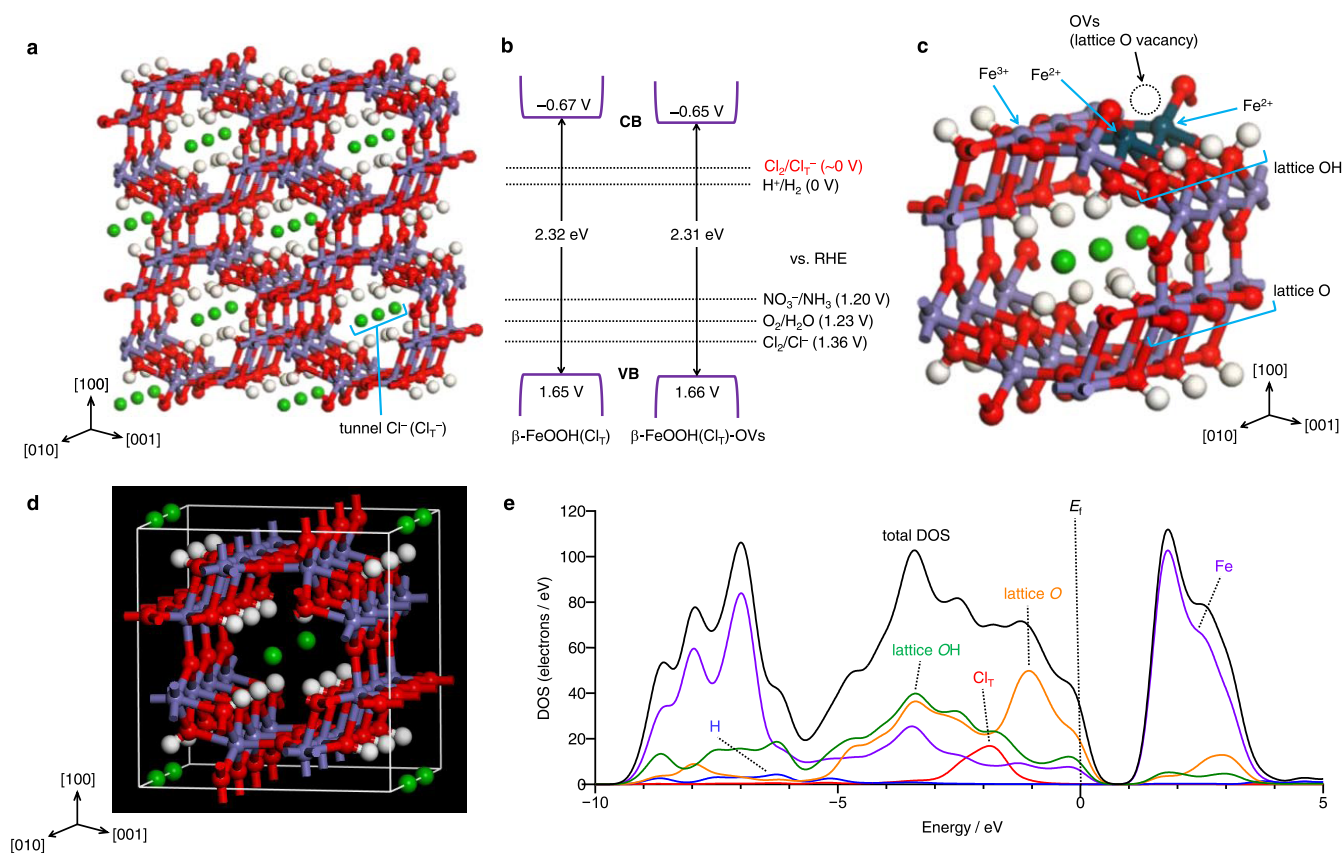
Figure 1. Crystal and electronic structures. (a) Crystal structure of β-FeOOH(Cl$_T$), where Fe^{3+}, O, H, and Cl$_T^-$ atoms are represented by purple, red, white, and light green spheres, respectively. (b) Electronic band structures of the catalysts. (c) Structure of the OVs on the (200) surface of β-FeOOH(Cl$_T$), where Fe^{2+} atoms are denoted by navy spheres. (d) Geometric structure of β-FeOOH(Cl$_T$) used for the DOS calculation, where the Cl–Cl distance along the [010] direction was set at 3.84 Å. (e) Total and partial DOS of the respective elements of β-FeOOH(Cl$_T$), where E_f denotes the Fermi level.

The optimal method for the NO$_3^-$-to-NH$_3$ reduction involves the treatment of strongly acidic NO$_3^-$-containing wastewater without neutralization using renewable energy sources and earth-abundant water as the reducing agent. Theoretically, semiconductor photocatalysis can promote the reduction of NO$_3^-$-to-NH$_3$ in water under sunlight and ambient conditions (eq 1). The photoformed valence band holes (h$_{VB}^+$) oxidize water to generate O$_2$ (eq 2), while the conduction band electrons (e$_{CB}^-$) reduce NO$_3^-$ to produce NH$_3$ (eq 3). Several photocatalysts have been used for NO$_3^-$ reduction,[18−20] but most of them reduced NO$_3^-$ to N$_2$ because this 5-electron reduction (eq 4) is thermodynamically more favorable than the 8-electron NO$_3^-$-to-NH$_3$ reduction (eq 3).[20,21]

$$HNO_3 + H_2O \rightarrow NH_3 + 2O_2 (\Delta G^\circ = +332 \text{ kJ mol}^{-1}) \tag{1}$$

$$2H_2O \rightleftharpoons O_2 + 4H^+ + 4e^- (E^\circ = +1.23 \text{ V vs NHE, pH 0}) \tag{2}$$

$$NO_3^- + 9H^+ + 8e^-$$
$$\rightarrow NH_3 + 3H_2O(E^\circ$$
$$= +1.20 \text{ V vs NHE, pH 0}) \tag{3}$$

$$NO_3^- + 6H^+ + 5e^-$$
$$\rightarrow \frac{1}{2}N_2 + 3H_2O(E^\circ$$
$$= +1.25 \text{ V vs NHE, pH 0}) \tag{4}$$
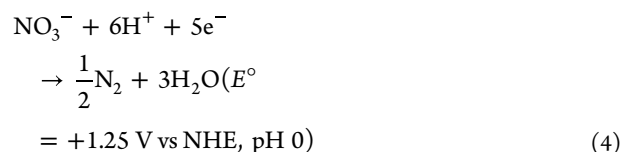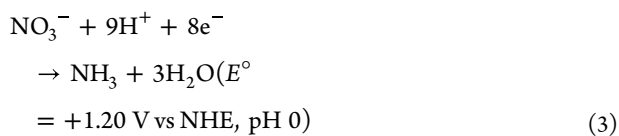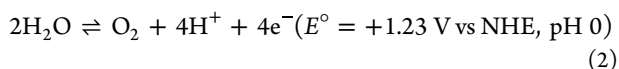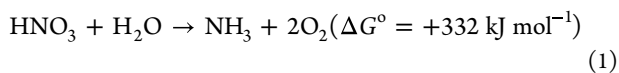
Recently, some photocatalysts have been demonstrated to promote the selective NO$_3^-$-to-NH$_3$ reduction, where surface oxygen vacancies (OVs) on a semiconductor (TiO$_2$),[22] metals (Cu,[23] Ag,[24] and Ru[25]), alloys (Pd−Cu[26] and Pd−Sn[27]), a metal oxide (BaO),[28] and a metal sulfide (FeS)[29] functioned as active sites for reduction. However, none of these systems promoted the reaction with water as the electron donor because of their low activity for water oxidation by h$_{VB}^+$ (eq 2), as demonstrated in water-splitting photocatalysis;[30,31] all of these systems required sacrificial electron donors such as methanol and formic acid. Therefore, developing a catalyst that can promote the selective NO$_3^-$-to-NH$_3$ reduction using water as the electron donor is crucial for achieving sustainable NH$_3$ synthesis.

Iron oxyhydroxides (goethite, akaganeite, lepidocrocite, and feroxyhyte) are naturally occurring minerals. Owing to their low cost, high chemical stability, and nontoxicity, they have been used as adsorbents,[32] sensors,[33] and electrocatalysts.[34] Among them, akaganeite (β-FeOOH(Cl$_T$)) forms a unique tunnel structure (Figure 1a): the four double chains of the Fe^{III}O$_3$(OH)$_3$ octahedra create tunnels along the [010] direction, which incorporate chloride anions (Cl$_T^-$) to
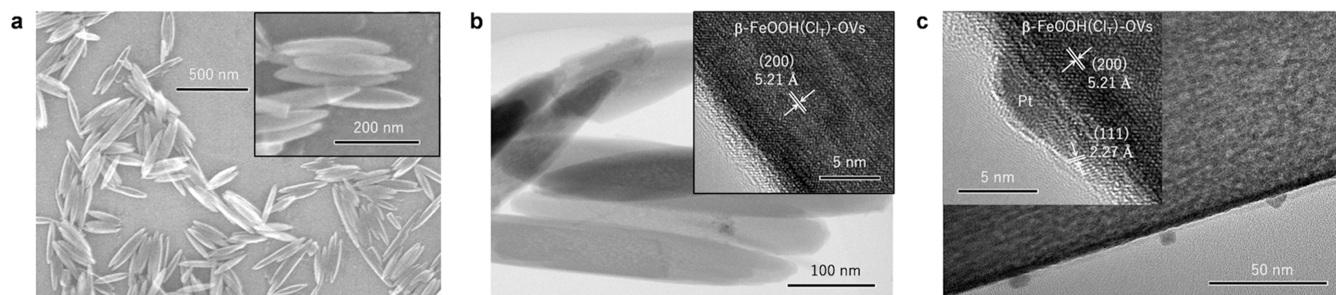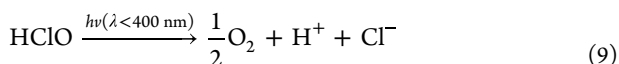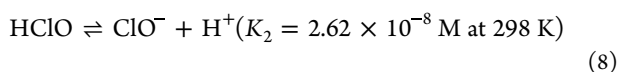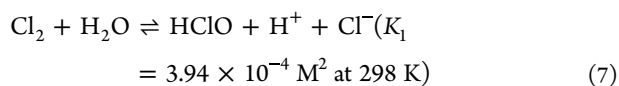
Figure 2. (a) SEM and (b) TEM images of β-FeOOH(Cl$_T$)-OVs. (c) TEM image of Pt-loaded β-FeOOH(Cl$_T$)-OVs prepared by the photodeposition method.

neutralize the positive charges. Despite its unique properties, no studies on the application of β-FeOOH(Cl$_T$) in photocatalysis have been reported. β-FeOOH(Cl$_T$) has a narrow band gap ($\sim$2.0 eV) and can be photoexcited under visible light ($\lambda < 600$ nm).[35] Notably, its density of states (DOS) near the valence bond (VB) maximum consists of hybridized two-point and three-point O 2p and Cl 3p orbitals. Thus, we hypothesized that the band gap photoexcitation of β-FeOOH(Cl$_T$) might promote self-oxidation of Cl$_T^-$ by h$_{VB}^+$, as observed for related Cl$^-$-containing semiconductors such as bismuth oxychlorides[36,37] and silver chloride.[38] The potential of Cl$^-$ self-oxidation for these semiconductors is more negative ($\sim$0 V vs RHE, eq 5) than that of water oxidation (+1.23 V vs a normal hydrogen electrode (NHE), eq 2).[37,38] This implies that the photoformed h$_{VB}^+$ on β-FeOOH(Cl$_T$) may be efficiently consumed by Cl$_T^-$ self-oxidation. Therefore, developing a system that can use water as the electron donor associated with Cl$_T^-$ self-oxidation by h$_{VB}^+$ and promote the selective NO$_3^-$-to-NH$_3$ reduction by e$_{CB}^-$ may cause a breakthrough for photocatalytic NH$_3$ generation.

$$2\beta\text{-FeOOH(Cl}_T) \rightarrow \text{Cl}_2 + 2\beta\text{-FeOOH}^+ + 2e^- (E = \sim 0 \text{ V vs RHE}) \quad (5)$$
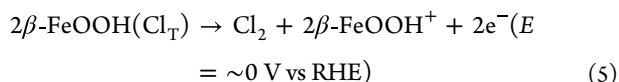
This study reports that β-FeOOH(Cl$_T$) containing OVs, when photoirradiated by UV light ($\lambda < 400$ nm) in strongly acidic NO$_3^-$ solutions containing Cl$^-$, successfully promotes the selective NO$_3^-$-to-NH$_3$ reduction with water. The OVs behaved as active sites for the NO$_3^-$-to-NH$_3$ reduction by e$_{CB}^-$ (eq 3), and h$_{VB}^+$ was consumed by Cl$_T^-$ self-oxidation to produce Cl$_2$ (eq 5). The Cl$^-$ in solution compensated for the eliminated Cl$_T^-$ (eq 6), promoting catalytic consumption of h$_{VB}^+$ by Cl$_T^-$. As expressed by eqs 7 and 8, Cl$_2$ formed in water is in equilibrium with hypochlorous acid (HClO),[39,40] with K_1 and K_2 being the equilibrium constants. HClO absorbs ultraviolet (UV) light and is decomposed into O$_2$ and Cl$^-$ (eq 9).[41] The successive cycle involving Cl$_T^-$ self-oxidation, Cl$_T^-$ compensation, and HClO photodecomposition stably promoted NO$_3^-$-to-NH$_3$ reduction with water (eq 1).

$$\beta\text{-FeOOH}^+ + \text{Cl}^- \rightarrow \beta\text{-FeOOH(Cl}_T) \quad (6)$$

$$\text{Cl}_2 + \text{H}_2\text{O} \rightleftharpoons \text{HClO} + \text{H}^+ + \text{Cl}^- (K_1 = 3.94 \times 10^{-4} \text{ M}^2 \text{ at 298 K}) \quad (7)$$

$$\text{HClO} \rightleftharpoons \text{ClO}^- + \text{H}^+ (K_2 = 2.62 \times 10^{-8} \text{ M at 298 K}) \quad (8)$$

$$\text{HClO} \xrightarrow{h\nu(\lambda<400 \text{ nm})} \frac{1}{2}\text{O}_2 + \text{H}^+ + \text{Cl}^- \quad (9)$$

RESULTS AND DISCUSSION

### Synthesis and Properties of Catalysts

Pristine β-FeOOH(Cl$_T$) was synthesized hydrothermally in water containing FeCl$_3$·6H$_2$O and KCl at 383 K.[42] β-FeOOH(Cl$_T$)-OVs was synthesized using ethylene glycol as the reducing agent to generate OVs (see Methods in Supporting Information).[37] Both β-FeOOH(Cl$_T$) and β-FeOOH(Cl$_T$)-OVs exhibited similar absorption bands up to $\sim$600 nm (Figure S1), and their band gap energies derived from the Tauc plots were $\sim$2.3 eV (Figure S2). The Mott–Schottky analysis of β-FeOOH(Cl$_T$) and β-FeOOH(Cl$_T$)-OVs (Figure S3) shows an n-type response with similar flat-band potentials (-0.67 and -0.65 V vs RHE, respectively). Therefore, these catalysts have similar electronic bands (Figure 1b). The powder X-ray diffraction (XRD) of both catalysts (Figure S4) shows peaks assigned to tetragonal β-FeOOH-(Cl$_T$) (JCPDS 80-1770). Scanning electron microscopy (SEM) observations of β-FeOOH(Cl$_T$)-OVs (Figure 2a) show barrel-shaped nanorods of $\sim$200 nm in length and $\sim$30 nm in diameter, similar to the morphology of β-FeOOH(Cl$_T$) (Figure S5).[42] Transmission electron microscopy (TEM) observation of β-FeOOH(Cl$_T$)-OVs (Figure 2b) exhibits a lattice spacing of 5.21 Å assigned to the (200) plane, indicating that these facets are exposed on the external surface of the nanorods.[42,43] The N$_2$ adsorption/desorption analysis of these catalysts shows a type-III isotherm (Figure S6) with low specific surface areas ($\sim$20 m^2 g^{-1}), suggesting that Cl$_T^-$ is incorporated within the tunnels (Figure 1a). These results indicate that the addition of ethylene glycol during hydrothermal synthesis barely affected the morphology, optical properties, and band structures of the catalysts.

X-ray photoelectron spectroscopy (XPS) was used to determine the surface composition of the catalysts (Figure S7). The Cl 2p spectra of both β-FeOOH(Cl$_T$) and β-FeOOH(Cl$_T$)-OVs (Figure S8) show peaks assigned to Cl$_T^-$ (196.6 and 198.1 eV).[44] The Fe 2p spectra of both catalysts (Figure S9) show Fe^{3+} peaks (709.2 and 722.8 eV) and Fe^{2+} peaks (711.7 and 725.0 eV) adjacent to the OVs.[44] The intensity of the Fe^{2+} peaks for β-FeOOH(Cl$_T$)-OVs was larger than that for β-FeOOH(Cl$_T$), indicating that the former contains more OVs. The O 1s spectra (Figure S10) exhibit peaks of lattice O (527.9 eV) and lattice OH (529.6 eV).[44] The intensity of the lattice O peak for β-FeOOH(Cl$_T$)-OVs was lower than that for β-FeOOH(Cl$_T$), suggesting that, as shown in Figure 1c, lattice O species are eliminated during the hydrothermal synthesis with ethylene glycol to create OVs. The surface elemental compositions of the catalysts (Fe, O, and Cl) were determined from the peak areas using atomic

Table 1. Surface Elemental Compositions of Catalysts[a]

entry	catalyst	composition (mol %)[b]			Fe species (%)[b]		O species (%)[c]	
		Fe	O	Cl	Fe^{3+}	Fe^{2+}	lattice OH	lattice O
1	β-FeOOH(Cl$_T$)	20.8	62.9	16.3	76.6	23.4	72.1	27.9
2	β-FeOOH(Cl$_T$)-OVs	24.1	58.5	17.4	63.6	36.4	85.1	14.9
3	β-FeOOH(Cl$_T$)-OVs after reaction in a pH 1.0 Cl$^-$-free solution[d]	26.8	62.6	10.6	65.0	35.0	83.9	16.1
4	β-FeOOH(Cl$_T$)-OVs after reaction in a pH 1.0 KCl solution[e]	25.4	57.8	16.8	62.5	37.5	84.1	15.9

[a]Determined from the XPS peak areas (Figures S8−S10) using atomic sensitivity factors (Fe 2p, 22.11; O 1s, 3.01; Cl 2p, 4.15). [b]Calculated from the XPS (Fe 2p) peak areas (Figure S9). [c]Calculated from the O 1a XPS (Figure S10). [d]After 24 h of photoirradiation (Figure 3a, orange). The pH of the solution was adjusted by adding HClO$_4$. [e]After 24 h of photoirradiation (Figure 3a, red). The pH of the solution was adjusted by adding HClO$_4$.
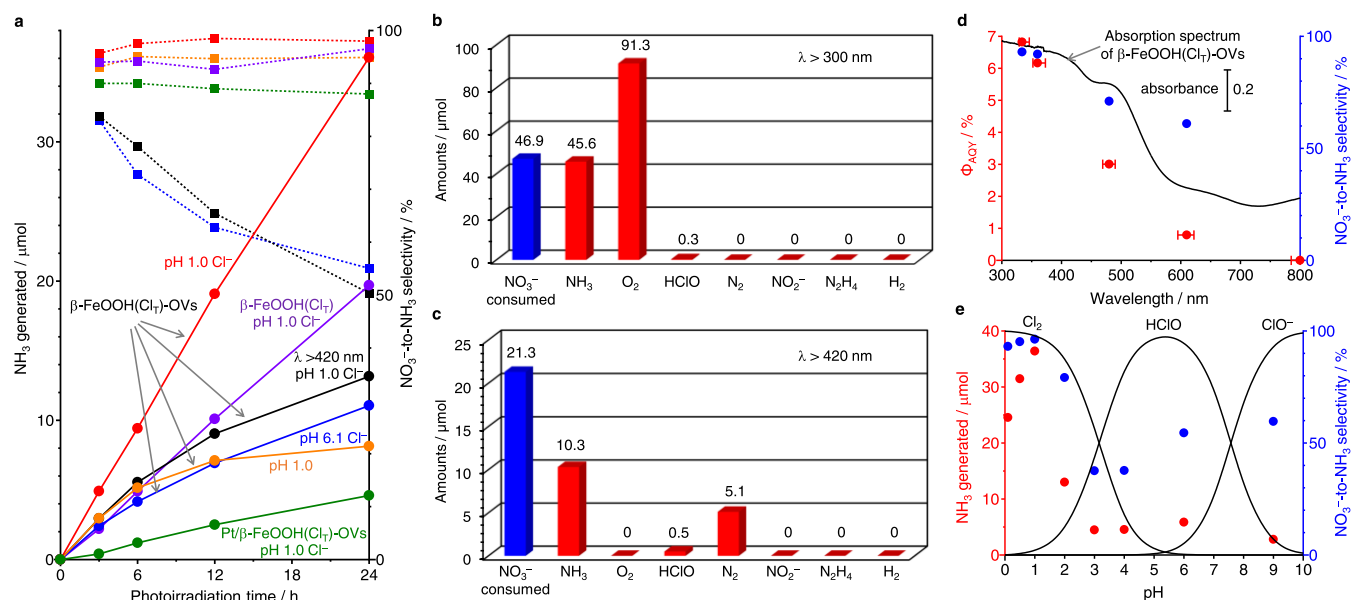

Figure 3. Photocatalytic properties. (a) Amounts of NH$_3$ generated (solid line) and selectivity for the NO$_3^-$-to-NH$_3$ reduction (dotted line) during photoirradiation [solution (0.1 L), catalyst (0.2 g), KNO$_3$ (1.0 mmol), Ar (0.3 L min^{-1}), λ > 300 nm (Xe lamp), and temperature (303 K)]. Amounts of NO$_3^-$ consumed and products generated after 24 h of (b) λ > 300 nm or (c) λ > 420 nm light irradiation with β-FeOOH(Cl$_T$)-OVs in a closed gas circulation system [pH 1.0 KCl solution (550 mM, 0.1 L), catalyst (0.2 g), KNO$_3$ (0.5 mmol), Ar (30 kPa), solar simulator, and temperature (303 K)]. (d) Action spectra for NH$_3$ generation over β-FeOOH(Cl$_T$)-OVs and selectivity for the NO$_3^-$-to-NH$_3$ reduction. (e) Effect of pH on the amount of NH$_3$ generated and the NO$_3^-$-to-NH$_3$ selectivity during 24 h of photoirradiation using β-FeOOH(Cl$_T$)-OVs, where the mole fraction distribution of the species (Cl$_2$, HClO, and ClO$^-$) is shown by the black lines.

sensitivity factors.[45] As shown in Table 1, the O content of β-FeOOH(Cl$_T$)-OVs (entry 2) was lower than that of β-FeOOH(Cl$_T$) (entry 1), which agrees with the higher Fe^{2+} content, confirming the formation of numerous OVs on β-FeOOH(Cl$_T$)-OVs. In addition, the lattice O content of β-FeOOH(Cl$_T$)-OVs (15%) was lower than that of β-FeOOH-(Cl$_T$) (28%), confirming that the OVs originated from lattice O vacancies (Figure 1c).

Photocatalysis

UV (λ < 400 nm) irradiation of β-FeOOH(Cl$_T$)-OVs in acidic solutions containing Cl$^-$ efficiently promoted the NO$_3^-$-to-NH$_3$ reduction. The photocatalytic activity was tested in KCl-containing KNO$_3$ solutions. The Cl$^-$ content of the solutions was set at 550 mM, which is similar to that in seawater.[46] The pH of the solutions was adjusted to ~1.0 using HClO$_4$ because ClO$_4^-$ is stable against oxidation or reduction[37] and scarcely affects the NO$_3^-$ reduction owing to its weak interaction with the OVs as mentioned later. A solution (0.1 L) containing the catalyst (0.2 g) and KNO$_3$ (1.0 mmol) was irradiated using a Xe lamp (λ > 300 nm) under magnetic stirring at 303 K and Ar gas bubbling. The emission spectrum of the lamp is presented

in Figure S11. Note that the pK_a of NH$_3$ is 9.3;[47] therefore, the NH$_3$ generated exists in the protonated NH$_4^+$ form. Figure 3a summarizes the change in the amount of NH$_3$ generated and the selectivity for the NO$_3^-$-to-NH$_3$ reduction over time under different conditions. As shown in red, λ > 300 nm light irradiation of β-FeOOH(Cl$_T$)-OVs in a pH 1.0 KCl solution linearly increased the amount of NH$_3$ generated with almost 100% NH$_3$ selectivity, indicating that the system stably promoted selective NO$_3^-$-to-NH$_3$ reduction. As shown in orange, the absence of KCl (pH 1.0 HClO$_4$ solution) also resulted in high NH$_3$ selectivity; however, the amount of NH$_3$ generated was saturated during photoirradiation, indicating that Cl$^-$ in the solution is necessary for stable NH$_3$ generation. As shown in blue, the photoreaction in a pH 6.1 KCl solution (without HClO$_4$ addition) exhibited low activity for NH$_3$ generation, and the NH$_3$ selectivity decreased with time. In addition, as shown in black, visible light (λ > 420 nm) irradiation of a pH 1.0 KCl solution also resulted in low NH$_3$ selectivity. Furthermore, as shown in purple, β-FeOOH(Cl$_T$) containing a low number of OVs showed high NH$_3$ selectivity similar to that of β-FeOOH(Cl$_T$)-OVs (red); however, the amount of NH$_3$ generated was considerably lower, suggesting
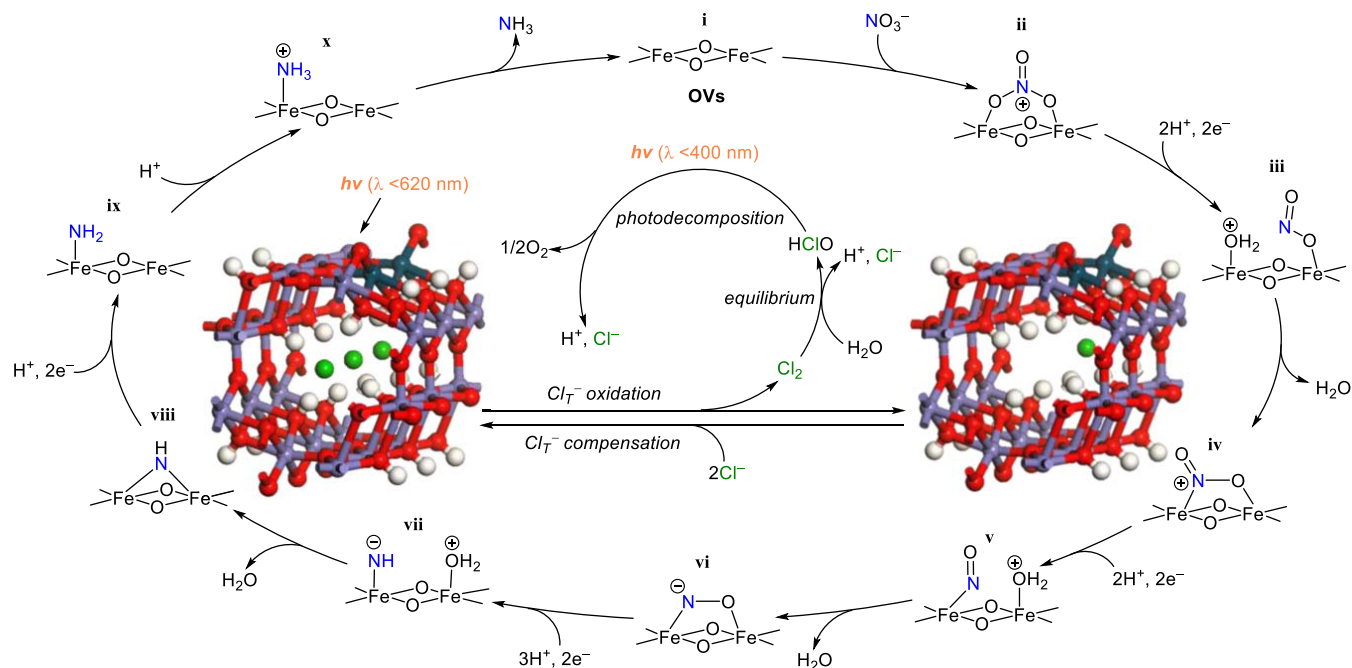
Figure 4. Proposed photocatalysis mechanism for the NO_3^--to-NH_3 reduction over β-FeOOH(Cl$_T$)-OVs with water as the electron donor. In-circle: water oxidation cycle; on-circle: NO_3^- reduction cycle.

that OVs are necessary for achieving high activity. These data indicate that UV irradiation ($\lambda < 400$ nm) of a catalyst containing numerous OVs in an acidic Cl$^-$ solution promotes efficient and selective NO_3^--to-NH_3 reduction.

UV irradiation of β-FeOOH(Cl$_T$)-OVs in a pH 1.0 KCl solution (without KNO$_3$) under N$_2$ bubbling did not produce NH$_3$ (Figure S12), indicating that the N source of the NH$_3$ generated was NO_3^-. This was further confirmed by the photoreactions using isotope-labeled K^{15}NO$_3$. A pH 1.0 KCl solution containing β-FeOOH(Cl$_T$)-OVs was photoirradiated with K^{14}NO$_3$ or K^{15}NO$_3$ for 48 h, and similar amounts of NH$_3$ were generated ($\sim$36 μmol). The solutions were treated with an indophenol assay,[37] and the resulting solutions with distinctive indophenol absorption at 630 nm were subjected to liquid chromatography-mass spectrometry (LC-MS) analysis (Figure S13). The K^{14}NO$_3$ sample shows an indophenol anion peak (m/z 198), whereas the K^{15}NO$_3$ sample shows a ^{15}N-labeled anion peak (m/z 199), verifying NO_3^- as the N source of the generated NH$_3$.

The β-FeOOH(Cl$_T$)-OVs system promotes the NO_3^--to-NH$_3$ reduction with water as the electron donor. Figure 3b summarizes the amounts of NO_3^- consumed and products generated during the photoirradiation of β-FeOOH(Cl)-OVs in a pH 1.0 KCl solution containing KNO$_3$ in a closed gas circulation system.[48] The amount of NO_3^- consumed was almost identical to that of NH$_3$ generated, where N$_2$, NO$_2^-$, N$_2$H$_4$, or H$_2$ was not detected, confirming the selective NO_3^--to-NH$_3$ reduction. Notably, the amount of O$_2$ generated was almost twice that of the NH$_3$ generated, confirming the quantitative NO_3^--to-NH$_3$ reduction with water (eq 1). The photocatalytic mechanism of β-FeOOH(Cl$_T$)-OVs in Cl$^-$ solutions is illustrated in Figure 4. As shown in the circle, e_{CB}^- reduces NO_3^- to NH$_3$ over the OVs. In contrast, as shown in the circle, h_{VB}^+ is consumed by Cl$_T^-$ self-oxidation to produce Cl$_2$ (eq 5). The Cl$^-$ in solution compensates for the eliminated Cl$_T^-$ (eq 6), promoting catalytic consumption of h_{VB}^+ by Cl$_T^-$. The Cl$_2$ formed in water is in equilibrium with

HClO (eq 7), which absorbs UV light and decomposes into O$_2$ and Cl$^-$ (eq 9). These successive cycles, consisting of Cl$_T^-$ self-oxidation by h_{VB}^+, Cl$_T^-$ compensation, and HClO photodecomposition, stably consume h_{VB}^+ with water as the electron donor in the entire system.

Cl$_T^-$ Oxidation/Compensation

The Cl$_T^-$ self-oxidation by h_{VB}^+ was confirmed using XPS. As listed in Table 1 (entries 2 and 3), the Cl content of β-FeOOH(Cl$_T$)-OVs decreased from 17.4 to 10.6 mol % upon photoirradiation in a pH 1.0 solution (without Cl$^-$), indicating the elimination of Cl$_T^-$ via oxidation. Under this condition (Figure 3a, orange), the NH$_3$ generation was saturated during photoirradiation. However, the addition of KCl to this solution regenerated NH$_3$ (Figure S14), indicating that Cl$^-$ in solution compensates for the eliminated Cl$_T^-$ and promotes the consumption of h_{VB}^+. In contrast, photoirradiation of β-FeOOH(Cl$_T$)-OVs in a pH 1.0 Cl$^-$ solution did not change the Cl content (Table 1, entry 4), and NH$_3$ was generated efficiently even after prolonged photoirradiation (Figure 3a, red). This indicates that the Cl$_T^-$ oxidation/compensation cycle (Figure 4, in-circle) promotes successive h_{VB}^+ consumption.

The Cl$_T^-$ self-oxidation by h_{VB}^+ is further confirmed by the DOS of β-FeOOH(Cl$_T$), which was determined by the density functional theory (DFT) calculations.[49] The calculations were performed using the structure in which four layers of the unit crystal were stacked in the [010] direction[50] (Figure 1d), where the lattice parameters of the unit crystal are presented in Table S1.[51] The total DOS (Figure 1e) and partial DOS of the respective elements (Figure S15) showed that the CB of β-FeOOH(Cl$_T$) comprised empty Fe 3d orbitals, whereas the VB consisted of O 2p and Cl 3p orbitals owing to the low electronegativity of Cl atoms.[50] This indicates that h_{VB}^+ is readily consumed by the Cl$_T^-$ self-oxidation, as observed for related Cl$^-$-containing semiconductors.[36–38]
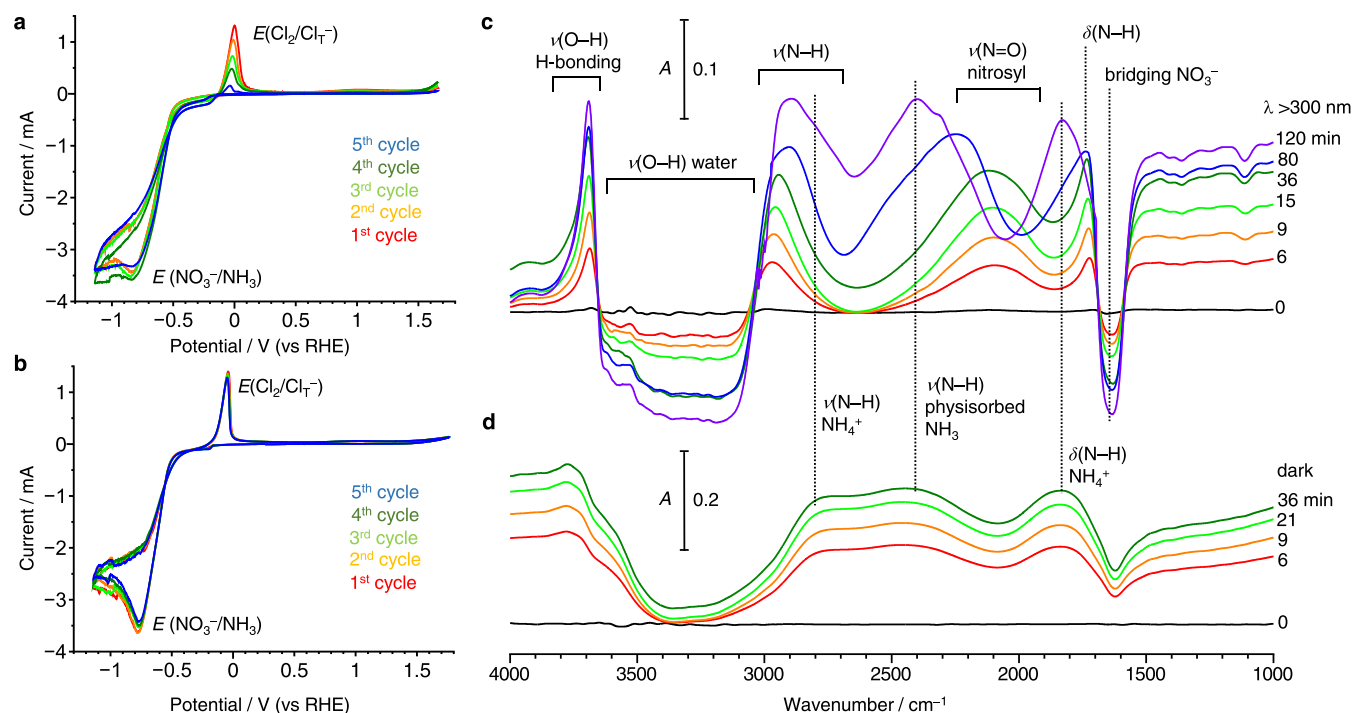
Figure 5. CV of β-FeOOH(Cl$_T$)-OVs measured with KNO$_3$ (10 mM) under Ar in (a) pH 1.0 KClO$_4$ solution (550 mM) and (b) pH 1.0 KCl solution (550 mM). Change in the diffuse-reflectance infrared Fourier transform spectra (DRIFTS) of (c) NO$_3^-$- and water-adsorbed β-FeOOH(Cl$_T$)-OVs under photoirradiation at 100 K in vacuo (0.9 Pa) and (d) NH$_3$ (40 Pa) gas adsorbed onto β-FeOOH(Cl$_T$)-OVs in the dark at 100 K.

The Cl$_T^-$ oxidation/compensation cycle was confirmed by photocurrent response measurements using a β-FeOOH(Cl$_T$)-OVs-loaded fluorine tin oxide (FTO) electrode (Figure S16). In the absence of Cl$^-$ in the solution, the current density decreased during repeated photoirradiation owing to the elimination of Cl$_T^-$ via oxidation. In contrast, in the presence of Cl$^-$, the current density was maintained during repeated cycles, indicating that the eliminated Cl$_T^-$ was compensated for from the solution, thus facilitating stable Cl$_T^-$ oxidation. Cyclic voltammetry (CV) analysis of the electrode further confirmed the Cl$_T^-$ oxidation/compensation cycle. The CV measured in a NO$_3^-$ solution without Cl$^-$ (Figure 5a) shows a cathodic current for NO$_3^-$ reduction (−0.5 V vs RHE) and an anodic current for Cl$_T^-$ oxidation (∼0 V vs RHE), as confirmed by the generation of NH$_3$ and HClO with the respective constant potentials. This indicates that Cl$_T^-$ oxidation occurs at a more negative potential than water oxidation (+1.23 V vs NHE, eq 2) and Cl$^-$ oxidation in the solution (>+1.36 V vs NHE, eq 10),[52] suggesting that Cl$_T^-$ oxidation efficiently consumes h$_{VB}^+$. However, in this case, the anodic current decreased during the cycles because of the Cl$_T^-$ consumption. In contrast, the CV measured with Cl$^-$ (Figure 5b) exhibited a stable anodic current, indicating that Cl$^-$ in solution successfully compensates for the eliminated Cl$_T^-$.

$$2Cl^- \rightarrow Cl_2 + 2e^- \quad (E^\circ = +1.36 \text{ V vs NHE, pH 0}) \quad (10)$$
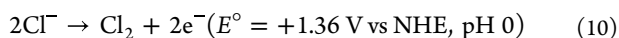
As shown in Figure 3a (orange), photoirradiation of β-FeOOH(Cl$_T$)-OVs in a pH 1.0 solution without Cl$^-$ for 24 h generated 8.1 μmol of NH$_3$, indicating that 64.8 μmol of Cl$_T^-$ was oxidized by h$_{VB}^+$ (eq 5). In contrast, 36.1 μmol of NH$_3$ was generated in the KCl solution (Figure 3a, red), indicating that 288.8 μmol of Cl$_T^-$ was oxidized. Thus, the turnover number for Cl$_T^-$ was estimated to be ∼5, indicating that the

Cl$_T^-$ oxidation/compensation cycle catalytically promoted the NO$_3^-$-to-NH$_3$ reduction. As shown in Figure S17, increasing the Cl$^-$ concentration in the solution enhanced NH$_3$ generation over β-FeOOH(Cl)-OVs, but the activity decreased when the Cl$^-$ concentration exceeded 1 M. The decreased activity may originate from the increased viscosity of the solution, which affects mass transfer during the reaction.[53] Therefore, solutions containing ∼500 mM Cl$^-$ are effective.

UV Irradiation

Cl$_2$ photoformed by h$_{VB}^+$ is in equilibrium with HClO (eq 7), which is photodecomposed into O$_2$ and Cl$^-$ (eq 9). Consequently, water functions as the electron donor in the entire system. UV (λ < 400 nm) irradiation is required for HClO photodecomposition because it only absorbs UV light.[41] As shown in Figure S18, λ > 420 nm light irradiation of an HClO solution barely decomposed HClO, whereas λ > 300 nm light irradiation promoted the stoichiometric decomposition of HClO into O$_2$ and Cl$^-$. The HClO photodecomposition by UV light is necessary for the selective NO$_3^-$-to-NH$_3$ reduction because HClO oxidizes the generated NH$_3$ into N$_2$ (eq 11).[54] Figure 3c shows the amounts of products after 24 h of λ > 420 nm light irradiation of β-FeOOH(Cl$_T$)-OVs in a pH 1.0 KCl solution. N$_2$ was also generated during the reaction with only 48% NO$_3^-$-to-NH$_3$ selectivity, whereas λ > 300 nm light irradiation (Figure 3b) exhibited 97% NO$_3^-$-to-NH$_3$ selectivity. In this case, the N balance {=([NH$_3$ generated] + 2 × [N$_2$ generated])/(NO$_3^-$ consumed) × 100} was 96%, and O$_2$ nor HClO was detected. This suggests that generated HClO reacts with NH$_3$ to produce N$_2$ (eq 11). Figure 3d shows the action spectrum of NH$_3$ generation over β-FeOOH(Cl$_T$)-OVs in a pH 1.0 KCl solution under monochromatic light irradiation. The apparent quantum yields
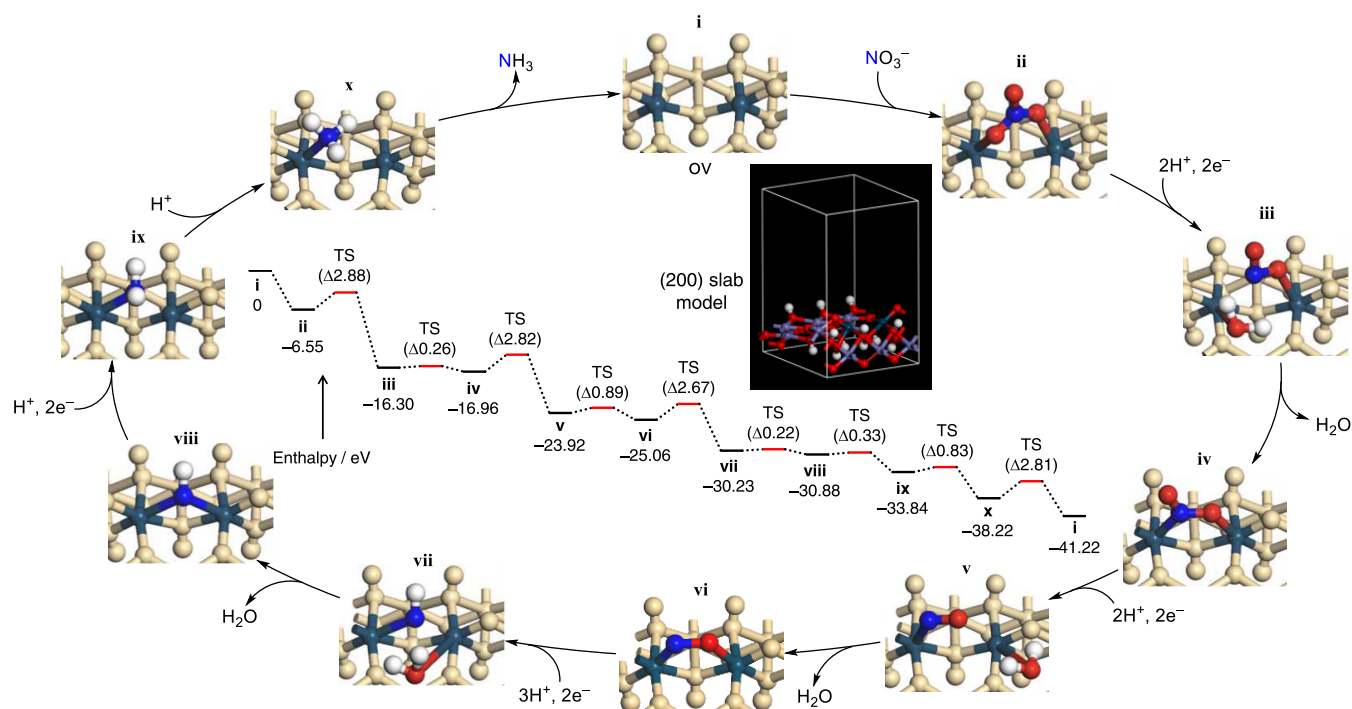
Figure 6. Proposed NO_3^--to-NH_3 reduction pathway and the corresponding potential energy profile. Calculations were performed on a (200) surface slab of β-FeOOH(Cl)-OVs (shown in the inset). The values in parentheses in the energy profile indicate the barriers (in eV) of the elementary steps.

(Φ_{AQY}) (red) agreed with the absorption spectrum of the catalyst, suggesting that the band gap photoexcitation generated NH_3. The NO_3^--to-NH_3 selectivity (blue) at 334 nm (93%) and 360 nm (92%) was high but decreased to 71% (480 nm) and 62% (610 nm) because visible light cannot decompose the generated HClO, leading to NH_3 decomposition (eq 11). These findings indicate that UV irradiation is necessary for HClO decomposition to suppress the subsequent decomposition of NH_3, even though the catalyst can be photoexcited by visible light up to ~600 nm.

$$2NH_4^+ + 3HClO \rightarrow N_2 + 5H^+ + 3Cl^- + 3H_2O \quad (11)$$
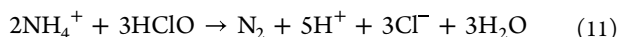
Acidic Conditions

Notably, acidic wastewater is favorable for efficient NH_3 generation (Figure 3a, red), whereas the reaction in a neutral (pH 6.1) KCl solution shows a lower NH_3 selectivity (blue). This is because, as expressed by eqs 7 and 8, the generated HClO exists stably at pH 3–7 and reacts with NH_3 to produce N_2, even though HClO is photodecomposed into both O_2 and Cl^- under UV irradiation. As shown in Figure S19, NH_3 decomposes easily when stirred in a NaClO solution with a neutral pH, whereas it is relatively stable at pH < 2. This indicates that at pH < 2, the HClO concentration decreases by equilibrium displacement and hinders NH_3 decomposition. Figure 3e shows the amounts of NH_3 generated and the NO_3^--to-NH_3 selectivity during the photoirradiation of β-FeOOH-(Cl_T)-OVs in KCl solutions with different pH values, where the mole fraction distributions of Cl_2, HClO, and ClO^- in the solution were calculated based on the equilibrium constants (eqs 7 and 8). At pH > 2, HClO exists stably and subsequently decomposes NH_3 (eq 11), resulting in low NH_3 selectivity. At pH < 2, the HClO concentration decreases and the NH_3 decomposition is suppressed, resulting in high NH_3 selectivity. The NH_3-generation activity was the highest at pH 1.0 and

decreased at lower pH values. This is because strongly acidic conditions decompose the catalyst (eq 12).[55] The photographs of the solutions containing β-FeOOH(Cl_T)-OVs after stirring at different pH values (Figure S20) show that the solutions are colorless at pH > 1 but turn yellowish brown at pH 0 or 0.5 due to Fe^{3+} generation. These findings indicate that acidic NO_3^- wastewater with a pH of 1–2 is favorable for NH_3 generation.

$$\beta\text{-FeOOH}(Cl_T) + 3H^+ \rightarrow Fe^{3+} + Cl^- + 2H_2O \quad (12)$$
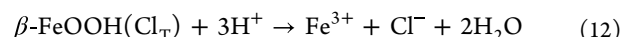
Role of Surface OVs

The OVs on the (200) facet of the rod surface (Figure 1c) functioned as reduction sites. As shown in Figure 3a, β-FeOOH(Cl_T)-OVs (red) generate a larger amount of NH_3 than β-FeOOH(Cl_T) (purple). The CV analysis (Figure S21) indicated that β-FeOOH(Cl_T)-OVs exhibit a larger current for NO_3^- reduction than β-FeOOH(Cl), which agrees with the larger number of lattice OVs (Table 1). To confirm that the OVs on the (200) surface serve as reduction sites, platinum (Pt) particles were loaded on β-FeOOH(Cl_T)-OVs by photodeposition,[56] involving photoirradiation of the catalyst in a KCl solution with $H_2PtCl_6 \cdot 6H_2O$. TEM observations (Figure 2c) show that Pt particles with diameters of ~5 nm were loaded onto the (200) rod surface, indicating that the OVs on the (200) surface reduced Pt^{4+} to form Pt particles. As shown in Figure 3a (green), when the Pt-loaded catalyst was used for the photoreaction in a pH 1.0 KCl solution, a considerably lower activity for NO_3^- reduction was observed than that of the bare catalyst (red). The Pt particles loaded create a Schottky barrier between the Pt–catalyst interface.[56] Accumulation of CB e^- on the Pt particles suppresses the donation of CB e^- to the OVs, thus decreasing the activity for NO_3^--to-NH_3 reduction on the OVs. The results confirm that
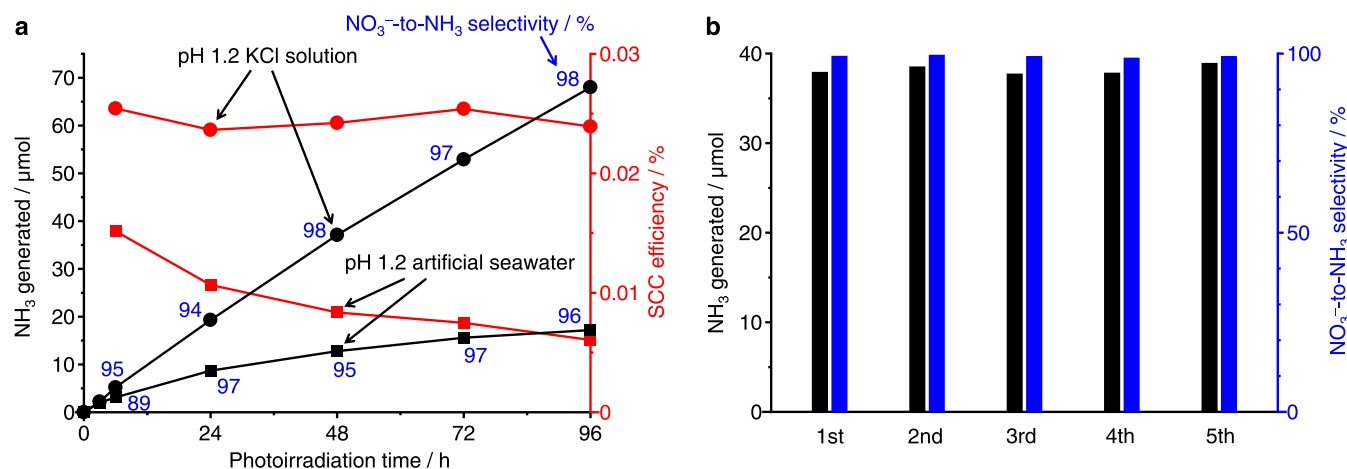
Figure 7. Artificial photosynthesis performance of β-FeOOH(Cl_T)-OVs. (a) Change in the amount of NH_3 generated and the SCC efficiency during photoreaction under simulated AM 1.5G sunlight (1 sun) irradiation [550 mM KCl solution or artificial seawater (100 mL), HNO_3 solution (13 M, 800 μM, 925 μmol), catalyst (0.2 g), Ar flow (0.3 L min^{-1}), and temperature (303 K)]. The blue numbers denote the NO_3^--to-NH_3 selectivity. (b) Results for repeated photoreactions with β-FeOOH(Cl_T)-OVs under AM1.5G simulated sunlight (1 sun). The catalyst after 96 h of photoreaction (a) was recovered by centrifugation and used for sequential photoreactions with the solution being replaced every 48 h of photoirradiation.

the OVs created on the (200) surface behave as sites for the NO_3^--to-NH_3 reduction.

The mechanism for the NO_3^--to-NH_3 reduction over the OVs is illustrated in Figure 4 (on-circle). Lewis-basic NO_3^- is adsorbed onto two Lewis-acidic Fe^{2+} sites adjacent to the OVs (i) with a bridging structure (ii).[22] N−O cleavage by e_{CB}^- (iii) and water removal produces a bridging NO_2 intermediate (iv). Subsequent N−O cleavage by e_{CB}^- (v) and water removal produces a bridging NO intermediate (vi). Further N−O cleavage by e_{CB}^- (vii), followed by water removal, forms a secondary amine intermediate (viii). Subsequent reduction by e_{CB}^- produces a primary amine intermediate (ix), and its protonation (x) decreases the Lewis basicity, causing desorption of NH_3 from the catalyst surface.

The DFT calculations (Figure 6) were performed on the (200) surface to confirm the proposed pathway. The (200) slab supercell (inset) was used for the calculations, where the unit crystal was stacked in three layers along the [010] direction and the (200) plane was cleaved, on which the OVs were created by removing lattice O. The steps (in-circle) show the potential energy surface of the intermediates (i−x) and transition states (TS) during the NO_3^--to-NH_3 reduction. The on-circle shows the intermediate structures, and the TS structures are shown in Figure S22. N−O cleavage by e_{CB}^- (ii → iii, iv → v, and vi → vii) and NH_3 desorption (x → (i)) are the rate-determining steps. The other steps such as NO_3^- adsorption (i → ii) and water removal (iii → iv, v → vi, and vii → viii) require negligible transition energies. As the reaction progresses, the intermediates lie at more negative levels. This indicates that the NO_3^--to-NH_3 reduction proceeds exothermically over the OVs, verifying the proposed pathway (Figure 4, on-circle). Notably, many photocatalytic systems promote the NO_3^--to-N_2 reduction (eq 4) more favorably,[18−21] which is thought to involve the desorption of NO_2^- (iii) or NO (v) intermediates from the surface, followed by the reduction of their coupling product (N_2O).[57] The stabilized intermediates (Figure 6) suggest their strong adsorption onto Lewis-acidic Fe^{2+} suppresses desorption, thus selectively promoting the NO_3^--to-NH_3 reduction.

In situ diffuse-reflectance infrared Fourier transform spectroscopy (DRIFTS) was used to confirm the proposed pathway. β-FeOOH(Cl_T)-OVs was stirred in a 1.0 M HNO_3 solution for 6 h, recovered by centrifugation, and dried at 353 K. Figure 5c shows the DRIFTS spectra of the NO_3^-- and water-adsorbed catalyst monitored under λ > 300 nm light irradiation in vacuo at 100 K. Photoirradiation decreased the stretching ν(O−H) band of adsorbed water (3000−3600 cm^{-1}). This suggests that water was transformed to O_2 via Cl_T^- self-oxidation followed by HClO photodecomposition (Figure 4, in-circle), as confirmed by the photoreaction result (Figure 3b). Simultaneously, the stretching band of NO_3^- with a bridging structure (1630 cm^{-1})[58] decreased, confirming the bridging adsorption mode of NO_3^- (ii). Additionally, a broad band at ~2100 cm^{-1} increased, which is assigned to the stretching ν(N═O) band of nitrosyl moieties,[59] confirming the formation of intermediates containing N═O bonds (iii−v). Furthermore, the stretching ν(N−H) (2800−2900 cm^{-1}) and bending δ(N−H) (1700−1900 cm^{-1}) bands increased,[60] indicating the formation of intermediates containing N−H bonds (vii−x). Prolonged photoirradiation produced a spectrum consisting of ν(N−H) and δ(N−H) bands for NH_4^+ and a ν(N−H) band for physisorbed NH_3,[60] which was similar to that of pure NH_3 adsorbed onto the catalyst (Figure 5d). These DFT calculations and DRIFTS results strongly support the stepwise NO_3^--to-NH_3 reduction pathway with water.

Solar-to-NH₃ Conversion

The artificial photosynthesis performance of the system was evaluated under practical conditions. Concentrated HNO_3 (~13 M, 800 μL) was added to a KCl solution (550 mM, 0.1 L). β-FeOOH(Cl_T)-OVs were dispersed in the resulting HNO_3 solution (93 mM, pH ~ 1.2) and photoirradiated by an AM1.5G simulated sunlight (1 sun).[61] As shown in Figure 7a (circle), photoirradiation increased the amount of NH_3 linearly with time even after 96 h, while maintaining almost 100% NO_3^--to-NH_3 selectivity. During prolonged photoirradiation, the solar-to-chemical conversion (SCC) efficiency was maintained at ~0.025%, indicating that the catalyst stably promoted the uphill reaction (eq 1). Furthermore, as shown in

Figure 7b, even after five reuse cycles, the recovered catalyst maintained its high activity and NO_3^--to-NH_3 selectivity. The diffuse-reflectance UV−visible spectrum (Figure S1) and XRD pattern (Figure S4) of the recovered catalyst were similar to those of the fresh catalyst. SEM images of the recovered catalyst (Figure S5) show barrel-shaped nanorods of ∼200 nm in length and ∼30 nm in diameter, similar to those of the fresh catalyst (Figure 2a). Moreover, the recovered and fresh catalysts have similar elemental (Fe, O, and Cl) compositions and Fe^{2+} and lattice O contents (Table 1). These findings indicate that the structure and activity of the catalyst were unchanged during the reaction, thus facilitating stable NO_3^--to-NH_3 reduction.

Seawater is a naturally abundant Cl^- solution; however, it is ineffective in the present system. As shown in Figure 7a (squares), the photoreaction in artificial seawater (∼550 mM Cl^-) generated a considerably smaller amount of NH_3 than that in the KCl solution (circles). This is because some anions (∼31 mM SO_4^{2-} and ∼2.7 mM HCO_3^-) in seawater suppress NO_3^- reduction despite their concentrations being lower than those of NO_3^- (93 mM). Seawater contains several cations (Na^+, K^+, Ca^{2+}, Mg^{2+}, and Sr^{2+}) and anions (SO_4^{2-}, HCO_3^-, and Br^-) in different amounts (Table S2).[62] To clarify the effect of these ions, photoreactions were performed in pH 1.0 KCl solutions containing each ion at concentrations similar to those in seawater (Figure S23). All cations and Br^- barely affected the NH_3-generation activity, whereas SO_4^{2-} and HCO_3^- significantly decreased the activity. CV analysis using β-$FeOOH(Cl_T)$-OVs-loaded FTO in a Cl^- solution with NO_3^- (Figure S24) indicated that the NO_3^- reduction current decreased by adding SO_4^{2-} or HCO_3^-, whereas the Cl_T^- oxidation current was unchanged, indicating that SO_4^{2-} and HCO_3^- suppress the NO_3^- reduction. This is because of the competitive adsorption of these Lewis-basic anions onto the OVs, which inhibits NO_3^- adsorption.[63] This was confirmed by surface DFT calculations using a (200) surface slab (Figure 6, inset). The adsorption enthalpies of NO_3^-, SO_4^{2-}, and HCO_3^- on the OVs were similar, whereas those of water and ClO_4^- were unstable (Figure S25).[64] This indicates that SO_4^{2-} and HCO_3^- are strongly adsorbed onto the OVs and inhibit NO_3^- adsorption, thereby suppressing the NO_3^- reduction. In addition, the present system requires O_2-free conditions; the photoreaction under airflow decreased the NH_3-generation activity (Figure S12) because O_2 is also strongly adsorbed on the OVs and suppresses NO_3^- reduction (Figure S25). The results indicate that the present system requires operation under SO_4^{2-}-, HCO_3^--, and O_2-free conditions. Nevertheless, the system can directly treat acidic NO_3^- wastewater without neutralization using inexpensive Cl^- salts and renewable solar energy under ambient conditions. Furthermore, several processes involving adsorption,[65] membrane,[66] and stripping technologies[67] have been used industrially for the separation/concentration of NH_3 in several kinds of solutions. A combination of these processes may enable the recovery of NH_3 generated by the present photoprocess although further investigations are necessary for practical applications because the separation/concentration efficiency may depend strongly on the pH and NH_3 and impurity concentrations of the solutions. Nevertheless, the combination of the photoprocess with these recovery processes will pave the way for sunlight-driven NO_3^--to-NH_3 transformation from wastewater and the separation/concentration of NH_3 for the upstream processes.

CONCLUSIONS

We demonstrated that UV irradiation of naturally occurring akaganeite powder with surface oxygen vacancies (β-FeOOH-(Cl_T)-OVs) in acidic Cl^- solutions catalyzes selective NO_3^--to-NH_3 reduction under ambient conditions. The photo-generated e_{CB}^- promoted the NO_3^--to-NH_3 reduction over the OVs, whereas h_{VB}^+ promoted Cl_T^- self-oxidation. The Cl^- in solution compensated for the eliminated Cl_T^-. Subsequent photodecomposition of generated HClO facilitated O_2 evolution. These Cl_T^- oxidation/compensation and HClO photodecomposition cycles facilitated stable NO_3^--to-NH_3 reduction using water as the electron donor. This photoprocess requires UV irradiation to decompose generated HClO, which causes subsequent oxidation of NH_3 to N_2. In addition, the reaction requires O_2-free conditions in solutions without certain anion impurities (SO_4^{2-} and HCO_3^-), which decrease the NH_3-generation activity. Nevertheless, the process can directly treat acidic NO_3^- wastewaters without neutralization and can be operated using an inexpensive akaganeite catalyst and low-cost Cl^- salts under ambient conditions. The presented concept, based on Cl_T^- oxidation/compensation for water oxidation and selective NO_3^--to-NH_3 reduction over OVs, may contribute to the sunlight-driven recycling of limited nitrogen resources.

EXPERIMENTAL SECTION

Synthesis of Catalysts

β-$FeOOH(Cl_T)$-OVs were prepared by the hydrothermal method as follows: $FeCl_3 \cdot 6H_2O$ (2.43 g, 9.0 mmol) and KCl (0.67 g, 9.0 mmol) were stirred in a mixture of water (42 mL) and ethylene glycol (6 mL) for 1 h at 298 K. The mixture was heated in a Teflon-lined stainless-steel autoclave at a rate of 1.5 K min^{-1} and a holding time of 12 h at 383 K. The resultant was recovered by centrifugation, washed with water and EtOH, and dried at 353 K for 3 h, affording yellow powders of β-$FeOOH(Cl_T)$-OVs. Pristine β-$FeOOH(Cl_T)$ was also prepared hydrothermally in total water (48 mL).[42] The Pt-loaded β-$FeOOH(Cl_T)$-OVs were prepared by a photodeposition method: β-$FeOOH(Cl_T)$-OVs (0.2 g) was dispersed in a KCl solution (550 mM, 0.1 L) containing $H_2PtCl_6 \cdot 6H_2O$ (7 mg). The tube was sealed using a rubber septum cap and photoirradiated with a Xe lamp for 24 h under magnetic stirring and Ar gas bubbling (0.3 L min^{-1}). The amount of Pt loaded was determined to be 0.60 wt % by X-ray fluorescence analysis.[38]

ASSOCIATED CONTENT

Ⓢ Supporting Information

The Supporting Information is available free of charge at https://pubs.acs.org/doi/10.1021/jacsau.4c00054.

> Methods, lattice parameters (Table S1), components in seawater (Table S2), characterization data of catalysts (Figures S1−S6), XPS (Figures S7−S10), light emission spectra (Figure S11), photoreaction results under different conditions (Figure S12), indophenol assay (Figure S13), photoreaction results without Cl^- (Figure S14), partial DOS (Figure S15), photocurrent response (Figure S16), effect of Cl^- amount (Figure S17), photodecomposition of HClO (Figure S18), effect of pH on the decomposition of NH_3 and catalyst (Figures S19 and S20), CV of catalyst (Figure S21), TS structures (Figure S22), effect of cations and anions on photocatalytic activity and CV (Figures S23 and S24), adsorption enthalpy of the respective adsorbates (Figure S25), and references (PDF)

■ AUTHOR INFORMATION

Corresponding Author

Yasuhiro Shiraishi − *Research Center for Solar Energy Chemistry and Division of Chemical Engineering, Graduate School of Engineering Science, Osaka University, Toyonaka 560-8531, Japan; Innovative Catalysis Science Division, Institute for Open and Transdisciplinary Research Initiatives (ICS-OTRI), Osaka University, Suita 565-0871, Japan;* ⬦ orcid.org/0000-0003-1812-0644;
Email: shiraishi.yasuhiro.es@osaka-u.ac.jp

Authors

Shotaro Akiyama − *Research Center for Solar Energy Chemistry and Division of Chemical Engineering, Graduate School of Engineering Science, Osaka University, Toyonaka 560-8531, Japan*

Wataru Hiramatsu − *Research Center for Solar Energy Chemistry and Division of Chemical Engineering, Graduate School of Engineering Science, Osaka University, Toyonaka 560-8531, Japan*

Kazutoshi Adachi − *Research Center for Solar Energy Chemistry and Division of Chemical Engineering, Graduate School of Engineering Science, Osaka University, Toyonaka 560-8531, Japan*

Satoshi Ichikawa − *Research Center for Ultra-High Voltage Electron Microscopy, Osaka University, Ibaraki 567-0047, Japan*

Takayuki Hirai − *Research Center for Solar Energy Chemistry and Division of Chemical Engineering, Graduate School of Engineering Science, Osaka University, Toyonaka 560-8531, Japan*

Complete contact information is available at:
https://pubs.acs.org/10.1021/jacsau.4c00054

Author Contributions

All authors contributed equally. CRediT: **Yasuhiro Shiraishi** conceptualization, project administration, supervision, visualization, writing-review & editing; **Shotaro Akiyama** data curation, formal analysis, investigation, writing-original draft; **Wataru Hiramatsu** data curation, formal analysis, investigation; **Kazutoshi Adachi** data curation, formal analysis, investigation; **Satoshi Ichikawa** formal analysis, investigation; **Takayuki Hirai** formal analysis, investigation, supervision.

Notes

The authors declare no competing financial interest.

■ REFERENCES

(1) Smil, V. Detonator of the population explosion. *Nature* **1999**, *400*, 415.

(2) Klerke, A.; Christensen, C. H.; Nørskov, J. K.; Vegge, T. Ammonia for hydrogen storage: challenges and opportunities. *J. Mater. Chem.* **2008**, *18*, 2304−2310.

(3) Humphreys, J.; Lan, R.; Tao, S. Development and Recent Progress on Ammonia Synthesis Catalysts for Haber−Bosch Process. *Adv. Energy Sustainable Res.* **2021**, *2*, No. 2000043.

(4) Li, M.; Huang, H.; Low, J.; Gao, C.; Long, R.; Xiong, Y. Recent Progress on Electrocatalyst and Photocatalyst Design for Nitrogen Reduction. *Small Methods* **2019**, *3*, No. 1800388.

(5) Wang, Z.; Hu, X.; Liu, Z.; Zou, G.; Wang, G.; Zhang, K. Recent Developments in Polymeric Carbon Nitride-Derived Photocatalysts and Electrocatalysts for Nitrogen Fixation. *ACS Catal.* **2019**, *9*, 10260−10278.

(6) Lin, S.; Zhang, X.; Chen, L.; Zhang, Q.; Mab, L.; Liu, J. A review on catalysts for electrocatalytic and photocatalytic reduction of N_2 to ammonia. *Green Chem.* **2022**, *24*, 9003.

(7) Klopper, W.; Ruscic, B.; Tew, D. P.; Biscoff, F. A.; Wolfsegger, S. Atomization energies from coupled-cluster calculations augmented with explicitly-correlated perturbation theory. *Chem. Phys.* **2009**, *356*, 14−24.

(8) Committee on Environmental Health & Committee on Infectious Diseases. Drinking Water From Private Wells and Risks to Children. *Pediatrics* **2009**, *123* (6), 1599−1605, DOI: 10.1542/peds.2009-0751.

(9) World Health Organization. *International Standards for Drinking Water*, 3rd ed.; Geneva: Switzerland, 1971.

(10) Katsounaros, I.; Dortsiou, M.; Kyriacou, G. Electrochemical reduction of nitrate and nitrite in simulated liquid nuclear wastes. *J. Hazard. Mater.* **2009**, *171*, 323−327.

(11) Lv, Y.-t.; Chen, X.; Zhang, X.; Zhu, C.; Pan, Y.; Sun, T.; Wang, L. Denitrification for acidic wastewater treatment: Long-term performance, microbial communities, and nitrous oxide emissions. *J. Biosci. Bioeng.* **2022**, *134*, 513−520.

(12) Duca, M.; Koper, M. T. M. Powering denitrification: the perspectives of electrocatalytic nitrate reduction. *Energy Environ. Sci.* **2012**, *5*, 9726−9742.

(13) Martínez, J.; Ortiz, A.; Ortiz, I. State-of-the-art and perspectives of the catalytic and electrocatalytic reduction of aqueous nitrates. *Appl. Catal., B* **2017**, *207*, 42−59.

(14) Stirling, A.; Papai, I.; Mink, J.; Salahub, D. R. Density functional study of nitrogen oxides. *J. Chem. Phys.* **1994**, *100*, 2910.

(15) Wang, Y.; Zhou, W.; Jia, R.; Yu, Y.; Zhang, B. Unveiling the Activity Origin of a Copper-based Electrocatalyst for Selective Nitrate Reduction to Ammonia. *Angew. Chem., Int. Ed.* **2020**, *59*, 5350−5354.

(16) Chen, F. Y.; Wu, Z. Y.; Gupta, S.; Rivera, D. J.; Lambeets, S. V.; Pecaut, S.; Kim, J. Y. T.; Zhu, P.; Finfrock, Y. Z.; Meira, D. M.; King, G.; Gao, G.; Xu, W.; Cullen, D. A.; Zhou, H.; Han, Y.; Perea, D. E.; Muhich, C. L.; Wang, H. Efficient conversion of low-concentration nitrate sources into ammonia on a Ru-dispersed Cu nanowire electrocatalyst. *Nat. Nanotechnol.* **2022**, *17*, 759−767.

(17) Gao, Q.; Pillai, H. S.; Huang, Y.; Liu, S.; Mu, Q.; Han, X.; Yan, Z.; Zhou, H.; He, Q.; Xin, H.; Zhu, H. Breaking adsorption-energy scaling limitations of electrocatalytic nitrate reduction on intermetallic CuPd nanocubes by machine-learned insights. *Nat. Commun.* **2022**, *13*, No. 2338, DOI: 10.1038/s41467-022-29926-w.

(18) Mori, T.; Suzuki, J.; Fujimoto, K.; Watanabe, M.; Hasegawa, Y. Reductive decomposition of nitrate ion to nitrogen in water on a unique hollandite photocatalyst. *Appl. Catal.* **1999**, *23*, 283−289.

(19) Adachi, M.; Kudo, A. Effect of Surface Modification with Layered Double Hydroxide on Reduction of Nitrate to Nitrogen over $BaLa_4Ti_4O_{15}$ Photocatalyst. *Chem. Lett.* **2012**, *41*, 1007−1008.

(20) Ren, H. T.; Jia, S. Y.; Zou, J. J.; Wu, S. H.; Han, X. A facile preparation of $Ag_2O/P25$ photocatalyst for selective reduction of nitrate. *Appl. Catal., B* **2015**, *176−177*, 53−61.

(21) Yang, W.; Wang, J.; Chen, R.; Xiao, L.; Shen, S.; Li, J.; Dong, F. Reaction mechanism and selectivity regulation of photocatalytic nitrate reduction for wastewater purification: progress and challenges. *J. Mater. Chem. A* **2022**, *10*, 17357−17376.

(22) Hirakawa, H.; Hashimoto, M.; Shiraishi, Y.; Hirai, T. Selective Nitrate-to-Ammonia Transformation on Surface Defects of Titanium Dioxide Photocatalysts. *ACS Catal.* 2017, 7, 3713−3720.

(23) Kominami, H.; Furusho, A.; Murakami, S.; Inoue, H.; Kera, Y.; Ohtani, B. Effective photocatalytic reduction of nitrate to ammonia in an aqueous suspension of metal-loaded titanium(IV) oxide particles in the presence of oxalic acid. *Catal. Lett.* 2001, 76, 31−34, DOI: 10.1023/A:1016771908609.

(24) Varapragasam, S. J. P.; Andriolo, J. M.; Skinner, J. L.; Grumstrup, E. M. Photocatalytic Reduction of Aqueous Nitrate with Hybrid Ag/g-C$_3$N$_4$ under Ultraviolet and Visible Light. *ACS Omega* 2021, 6, 34850−34856, DOI: 10.1021/acsomega.1c05523.

(25) Hao, D.; Ren, J.; Wang, Y.; Arandiyan, H.; Garbrecht, M.; Bai, X.; Shon, K. Wei.; Jie, Ni. B. A Green Synthesis of Ru Modified g-C$_3$N$_4$ Nanosheets for Enhanced Photocatalytic Ammonia Synthesis. *Energy Mater. Adv.* 2021, 2021, No. 9761263, DOI: 10.34133/2021/9761263.

(26) Yamauchi, M.; Abe, R.; Tsukuda, T.; Kato, K.; Takata, M. Highly Selective Ammonia Synthesis from Nitrate with Photocatalytically Generated Hydrogen on CuPd/TiO$_2$. *J. Am. Chem. Soc.* 2011, 133, 1150−1152.

(27) Tong, N.; Wang, Y.; Liu, Y.; Li, M.; Zhang, Z.; Huang, H.; Sun, T.; Yang, J.; Li, F.; Wang, X. PdSn/NiO/NaTaO$_3$: La for photocatalytic ammonia synthesis by reduction of NO$_3$ with formic acid in aqueous solution. *J. Catal.* 2018, 361, 303−312.

(28) Li, J.; Chen, R.; Wang, J.; Zhou, Y.; Yang, G.; Dong, F. Subnanometric alkaline-earth oxide clusters for sustainable nitrate to ammonia photosynthesis. *Nat. Commun.* 2022, 13, No. 1098.

(29) Choi, H.; Peters, A. W.; Noh, H.; Gallington, L. C.; Platero-Prats, A. E.; DeStefano, M. R.; Rimoldi, M.; Goswami, S.; Chapman, K. W.; Farha, O. K.; Hupp, J. T. Vapor-Phase Fabrication and Condensed-Phase Application of a MOF-Node-Supported Iron Thiolate Photocatalyst for Nitrate Conversion to Ammonium. *ACS Appl. Energy Mater.* 2019, 2, 8695−8700.

(30) Kudo, A.; Miseki, Y. Heterogeneous photocatalyst materials for water splitting. *Chem. Soc. Rev.* 2009, 38, 253−278.

(31) Hisatomi, T.; Domen, K. Reaction systems for solar hydrogen production via water splitting with particulate semiconductor photocatalysts. *Nat. Catal.* 2019, 2, 387−399.

(32) Chitrakar, R.; Tezuka, S.; Sonoda, A.; Sakane, K.; Ooi, K.; Hirotsu, T. Phosphate adsorption on synthetic goethite and akaganeite. *J. Colloid Interface Sci.* 2006, 298, 602−608.

(33) Marinho, J. Z.; Montes, R. H. O.; Moura, A. P.; Longo, E.; Varela, J. A.; Munoz, R. A. A.; Lima, R. C. Rapid preparation of a-FeOOH and a-Fe$_2$O$_3$ nanostructures by microwave heating and their application in electrochemical sensors. *Mater. Res. Bull.* 2014, 49, 572−576, DOI: 10.1016/j.materresbull.2013.09.052.

(34) Jung, J.; Song, K.; Bae, D.; Lee, S.; Lee, G.; Kang, Y. β-FeOOH nanorod bundles with highly enhanced round-trip efficiency and extremely low overpotential for lithium-air batteries. *Nanoscale* 2013, 5, 11845.

(35) Zhang, D.; Han, X.; Kong, X.; Zhang, F.; Lei, X. The Principle of Introducing Halogen Ions Into β-FeOOH: Controlling Electronic Structure and Electrochemical Performance. *Nano-Micro Lett.* 2020, 12, No. 107, DOI: 10.1007/s40820-020-00440-2.

(36) Fujito, H.; Kunioku, H.; Kato, D.; Suzuki, H.; Higashi, M.; Kageyama, F.; Abe, R. Layered Perovskite Oxychloride Bi$_4$NbO$_8$Cl: A Stable Visible Light Responsive Photocatalyst for Water Splitting. *J. Am. Chem. Soc.* 2016, 138, 2082−2085.

(37) Shiraishi, Y.; Hashimoto, M.; Chishiro, K.; Moriyama, K.; Tanaka, S.; Hirai, T. Photocatalytic Dinitrogen Fixation with Water on Bismuth in Chloride Solutions for Solar-to-Chemical Energy Conversion. *J. Am. Chem. Soc.* 2020, 142, 7574−7583.

(38) Shiraishi, Y.; Shimabukuro, Y.; Shima, K.; Ichikawa, S.; Tanaka, S.; Hirai, T. Sunlight-driven generation of hypochlorous acid on plasmonic Au/AgCl catalyst in aerated chloride solution. *JACS Au* 2023, 3, 1403−1412.

(39) Connick, R. E.; Chia, Y. T. The hydrolysis of chlorine and its variation with temperature. *J. Am. Chem. Soc.* 1959, 81, 1280−1284.

(40) Czarnetzki, L. R. Aspects of Electrochemical Production of Hypochlorite and Chlorate. In *Technische Universiteit Eindhoven*; Eindhoven, 1989.

(41) Watts, M. J.; Linden, K. G. Chlorine photolysis and subsequent OH radical production during UV treatment of chlorinated water. *Water Res.* 2007, 41, 2871−2878.

(42) Liang, Y.; Yu, Y.; Huang, Y.; Shia, Y.; Zhang, B. Adjusting the electronic structure by Ni incorporation: a generalized in situ electrochemical strategy to enhance water oxidation activity of oxyhydroxides. *J. Mater. Chem. A* 2017, 5, 13336.

(43) Liu, Q.; Liu, Q.; Xie, L.; Ji, Y.; Li, T.; Zhang, B.; Li, N.; Tang, B.; Liu, Y.; Gao, S.; Luo, Y.; Yu, L.; Kong, Q.; Sun, X. High-Performance Electrochemical Nitrate Reduction to Ammonia under Ambient Conditions Using a FeOOH Nanorod Catalyst. *ACS Appl. Mater. Interfaces* 2022, 14, 17312−17318.

(44) Kim, B. G.; Park, J.; Choi, W.; Han, D. S.; Kim, J.; Park, H. Electrocatalytic arsenite oxidation using iron oxyhydroxide polymorphs (α-, β-, and γ-FeOOH) in aqueous bicarbonate solution. *Appl. Catal., B* 2021, 283, No. 119608.

(45) Scofield, J. H. Hartree-Slater Subshell Photoionization Cross-Sections at 1254 and 1487 eV. *J. Electron Spectrosc. Relat. Phenom.* 1976, 8, 129−137.

(46) Mase, K.; Yoneda, M.; Yamada, Y.; Fukuzumi, S. Seawater usable for production and consumption of hydrogen peroxide as a solar fuel. *Nat. Commun.* 2016, 7, No. 11470.

(47) Stumm, W.; Morgan, J. J. *Aquatic Chemistry: Chemical Equilibria and Rates in Natural Waters*, 3rd ed.; John Wiley & Sons: New York, 1996.

(48) Shiraishi, Y.; Ueda, Y.; Soramoto, A.; Hinokuma, S.; Hirai, T. Photocatalytic hydrogen peroxide splitting on metal-free powders assisted by phosphoric acid as a stabilizer. *Nat. Commun.* 2020, 11, No. 3386.

(49) Clark, S. J.; Segall, M. D.; Chris, J. P.; Phill, J. H.; Matt, I. J. P.; Keith, R.; Mike, C. P. Z. First principles methods using CASTEP. *Z. Kristallogr. - Cryst. Mater.* 2005, 220, 567−570, DOI: 10.1524/zkri.220.5.567.65075.

(50) Huang, Z.; Guan, X.; Li, M.; Guo, L. First-Principles Investigation of β-FeOOH for Hydrogen Evolution: Identifying Reactive Sites and Boosting Surface Reactions. *Chem. - Eur. J.* 2020, 26, 7118−7123.

(51) Post, J. E.; Peter, J. H.; Robert, B. V. D.; Jonathan, C. H. Neutron and temperature-resolved synchrotron X-ray powder diffraction study of akaganéite. *Am. Mineral.* 2003, 88, 782−788.

(52) Du, J.; Chen, Z.; Chen, C.; Meyer, T. J. A Half-Reaction Alternative to Water Oxidation: Chloride Oxidation to Chlorine Catalyzed by Silver Ion. *J. Am. Chem. Soc.* 2015, 137, 3193−3196.

(53) Lin, J.; Li, Y.; Xie, B. Heterogeneous photocatalytic performances of CO$_2$ reduction based on the [Emim]BF$_4$ + TEOA + H$_2$O system. *RSC Adv.* 2019, 9, 35841−35846.

(54) Zhang, Y.; Li, J.; Bai, J.; Li, L.; Chen, S.; Zhou, T.; Wang, J.; Xia, L.; Xu, Q.; Zhou, B. Extremely Efficient Decomposition of Ammonia N to N$_2$ Using ClO$^{•}$ from Reactions of HO$^{•}$ and HOCl Generated in Situ on a Novel Bifacial Photoelectroanode. *Environ. Sci. Technol.* 2019, 53, 6945−6953.

(55) Rubio, J.; Matijevic, E. Interactions of Metal Hydrous Oxides with Chelating Agents. I. β-FeOOH-EDTA. *J. Colloid Interface Sci.* 1979, 68, 408−421.

(56) Wenderich, K.; Mul, G. Methods, Mechanism, and Applications of Photodeposition in Photocatalysis: A Review. *Chem. Rev.* 2016, 116, 14587−14619.

(57) Zhang, R.; Shuai, D.; Guy, K. A.; Shapley, J. R.; Strathmann, T. J.; Werth, C. J. Elucidation of Nitrate Reduction Mechanisms on a Pd-In Bimetallic Catalyst using Isotope Labeled Nitrogen Species. *ChemCatChem* 2013, 5, 313−321.

(58) Westerberg, B.; Fridell, E. A transient FTIR study of species formed during NO$_x$ storage in the Pt/BaO/Al$_2$O$_3$ system. *J. Mol. Catal. A: Chem.* 2001, 165, 249−263.

(59) Weingand, T.; Kuba, S.; Hadjiivanov, K.; Knözinger, H. Nature and reactivity of the surface species formed after NO adsorption and

NO + O$_2$ coadsorption on a WO$_3$-ZrO$_2$ catalyst. *J. Catal.* **2002**, *209*, 539−546.

(60) Guntida, A.; Suriye, A.; Panpranot, J.; Praserthdam, P. Comparative Study of Lewis Acid Transformation on Non-reducible and Reducible Oxides Under Hydrogen Atmosphere by In Situ DRIFTS of Adsorbed NH$_3$. *Top. Catal.* **2018**, *61*, 1641−1652.

(61) Gordon, I.; Krebs, F. C.; Mathew, X.; Lampert, C. M.; Rougier, A.; Smestad, G. P.; Subrahmanyam, A. Editorial. *Sol. Energy Mater. Sol. Cells* **2015**, *133*, A1−A6.

(62) Zidouri, H. Desalination in Morocco and presentation of design and operation of the Laayoune seawater reverse osmosis plant. *Desalination* **2000**, *131*, 137−145.

(63) Schneider, W. F. Qualitative Differences in the Adsorption Chemistry of Acidic (CO$_2$, SO$_x$) and Amphiphilic (NO$_x$) Species on the Alkaline Earth Oxides. *J. Phys. Chem. B* **2004**, *108*, 273−282.

(64) Otte, K.; Wolfgang, W. S.; Pentcheva, R. Density functional theory study of water adsorption on FeOOH surfaces. *Surf. Sci.* **2012**, *606*, 1623−1632.

(65) Cruz, H.; Ying, Y. L.; Guest, J. S.; Rabaey, K.; Batstone, D.; Laycock, B.; Verstraete, W.; Pikaar, I. Mainstream ammonium recovery to advance sustainable urban wastewater management. *Environ. Sci. Technol.* **2019**, *53*, 11066−11079.

(66) Ye, Y.; Ngo, H. H.; Guo, W.; Liu, Y.; Chang, S. W.; Nguyen, D. D.; Liang, H.; Wang, J. A critical review on ammonium recovery from wastewater for sustainable wastewater management. *Bioresour. Technol.* **2018**, *268*, 749−758.

(67) Lorick, D.; Macura, B.; Ahlström, M.; Grimvall, A.; Harder, R. Effectiveness of struvite precipitation and ammonia stripping for recovery of phosphorus and nitrogen from anaerobic digestate: a systematic review. *Environ. Evidence* **2020**, *9*, No. 27, DOI: 10.1186/s13750-020-00211-x.